



## Generation and decoherence of soliton spatial superposition states

Abhijit Pendse,<sup>1,\*</sup> Shruti Shirol,<sup>1,2</sup> Shivakant Tiwari<sup>1</sup> ,<sup>1</sup> and Sebastian Wüster<sup>1,†</sup> 

<sup>1</sup>*Department of Physics, Indian Institute of Science Education and Research, Bhopal, Madhya Pradesh 462 066, India*

<sup>2</sup>*Department of Physics, University of Massachusetts-Amherst, Amherst, Massachusetts 01003, USA*



(Received 28 July 2020; accepted 15 October 2020; published 30 November 2020)

Due to their coherence properties, dilute atomic gas Bose-Einstein condensates seem a versatile platform for controlled creation of mesoscopically entangled states with a large number of particles and allow controlled studies of their decoherence. However, the creation of such states intrinsically involves many-body quantum dynamics that cannot be captured by mean-field theory and, thus, invalidates the most common methods for the description of condensates. We follow up on a proposal in which a condensate cloud as a whole is brought into a superposition of two different spatial locations by mapping entanglement from a strongly interacting Rydberg atomic system onto the condensate using off-resonant laser dressing [*Phys. Rev. Lett.* **115** 040401 (2015)]. A variational many-body ansatz akin to recently developed multiconfigurational methods allows us to model this entanglement mapping step explicitly, while still preserving the simplicity of mean-field physics for the description of each branch of the superposition. In the second part of the article, we model the decoherence process due to atom losses in detail. Altogether we confirm earlier estimates that tightly localized clouds of 400 atoms can be brought into a quantum superposition of two locations about 3  $\mu\text{m}$  apart and remain coherent for about 1 ms.

DOI: [10.1103/PhysRevA.102.053322](https://doi.org/10.1103/PhysRevA.102.053322)

### I. INTRODUCTION

Ever since the formulation of quantum mechanics in the 1920s, the quantum to classical transition has been the subject of intense study [1–6]. One apparent difference between the quantum and the classical realms is the existence of quantum coherent superposition states in the former. Decoherence can explain within the usual framework of quantum mechanics why these are typically not observed for macroscopic systems, whereas the root cause for observing a definite measurement outcome is still not satisfactorily explained within the theory [1]. This motivates the formulation of collapse models [7,8], that explore if additional physical laws cause apparently different behavior of quantum and classical objects.

The unsatisfactory understanding of the quantum to classical transition motivates an experimental drive to bring ever larger controllable quantum systems into superposition states, to check whether they adhere to standard decoherence theory and, hence, to the usual framework of quantum mechanics or whether new physics comes into play. Although the creation of truly macroscopic quantum systems remains elusive [9], mesoscopic settings that are pushing towards this frontier include matter wave interference in  $\text{C}_{60}$  molecules [10], organic molecules [11,12] or superposition of currents in superconductors [13]. In atomic systems, superposition states involving up to 20 qubits have been realized for trapped neutral atoms [14] and up to 14 qubits for trapped ions [15,16]. There are further proposals to enlarge this pool of candidate platforms for the exploration of the quantum classical boundary through

the generation of mesoscopically entangled states in cavity optomechanical systems [17], photon fields in a Kerr medium [18], Rydberg dressed atom clouds [19], and in Bose-Einstein condensates (BECs) [20–26]. Finally, mesoscopic superposition states also have technological applications in quantum metrology where they allow measurements beyond the standard quantum limit [27].

Here we explore a scheme to generate quantum superposition state of a gaseous BEC that was proposed in Ref. [22] in more detail where a mesoscopic superposition state of a matter wave bright soliton [28–43] would be prepared by first entangling two control atoms exploiting the Rydberg blockade [44–47] and then mapping this entanglement onto the bright soliton using Rydberg dressed long-range interactions [22,48–56]. Initially, a single stationary bright soliton forms a quasi-one-dimensional (1D) BEC flanked by two control atoms trapped on either side of it. One then attempts to optically excite these control atoms into a Rydberg state. Since the interaction blockade prohibits simultaneous excitation of both control atoms, this generates an entangled Bell state where either the one or the other control atom has been excited. Only at this point is the entire soliton subjected to Rydberg dressing such that it is accelerated away from the excited control atom. Since the system was in a superposition state of either control atom excited, the soliton will evolve into a superposition state of different velocities and later different positions.

The first aspect of the above scheme that we describe here in more detail, is the transfer of entanglement from the control atoms onto the mesoscopic BEC bright soliton. Once the latter is in a genuine entangled state, it can no longer be dealt with using mean-field theory in which all the condensate particles macroscopically occupy the same single-particle state. To nonetheless model the mapping step, we

\*apendse@iiserb.ac.in

†sebastian@iiserb.ac.in

employ a variational many-body ansatz. For that we assume that the total state of control atoms and Bose gas may be a superposition in which each state of the control atom system is entangled with a separate highly occupied orbital for the Bose gas. This scheme goes beyond the standard mean-field Gross-Pitaevskii dynamics by allowing entanglement arising from the interaction of the BEC soliton with the control atoms. Our approach has been guided by recent developments of the multilayer multiconfigurational time-dependent Hartree for bosons (ML-MCTDHB) [57–60] used to describe the dynamics of composite systems, each with multiple states. Compared to this technique, we keep the ansatz used here as simple as possible to describe the physics of interest to us. A similar approach was used, e.g., in Ref. [61].

The second aspect of the experiment proposed in Ref. [22] that we expand upon here is decoherence of the mesoscopic superposition state after it is created. We expect the primary source of decoherence in this scenario to be atom loss, which can be classified into one-, two-, and three-body losses [62–66]. Here, we use a Lindblad master equation [67] to explicitly model the effect of these loss processes on the entangled state of a BEC soliton, assuming a simplified two-mode model for its spatial dynamics. As is known, the decay of a single atom from the entangled state would destroy the entanglement, hence, the combination of all loss processes will govern the timescale on which the mesoscopic entanglement can be sustained [68,69].

An advantage of the present superposition state generation scheme is the degree of control over the mesoscopic entanglement generation process. By choosing the Rydberg state of the control atoms and the Rydberg state to which the BEC is dressed, one can control the duration of the required interaction step as well as the final velocity of the soliton. Simultaneously, also the range of Rydberg-Rydberg interactions and, thus, the spatial extent of the superposition state can be adjusted. This sets it apart from other proposals to create mesoscopic superposition states in BECs using the collision between two solitons [20], scattering of solitons from a barrier [21] or collision between different condensates [23,24].

This paper is organized as follows. We start in Sec. II with a review of the entanglement transfer scheme proposed in Ref. [22]. After defining the model and Hamiltonian in Sec. II A, we then describe our many-body ansatz for modeling the generation of a superposition state of soliton locations and present the resultant equations of motions in Sec. II B, whereas details of the derivation are deferred to Appendix A. For experimentally relevant parameters, listed fully in Appendix B, we then present our numerical simulations in Sec. II C. After Sec. II has, thus, comprehensively treated the generation of a soliton spatial superposition state, we then move to its destruction by decoherence in Sec. III using a Lindblad master equation parameters of which are derived in Appendix C. We conclude the article with a discussion of the possible future directions.

## II. ENTANGLEMENT MAPPING

Let us now briefly review the scheme for the creation of a spatial superposition state of a BEC bright soliton proposed in Ref. [22] in more detail. Consider an initially stationary bright

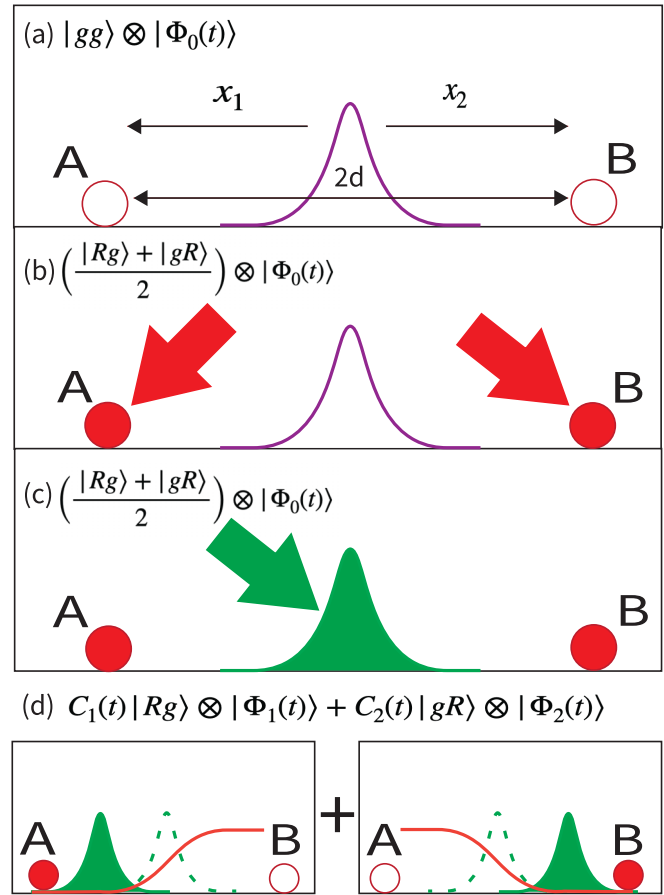


FIG. 1. Generating a mesoscopically entangled state of a BEC bright soliton state by entanglement transfer from a pair of control atoms as proposed in Ref. [22]. The purple curved line sketches the density profile of the soliton and the circles marked A and B represent control atoms. (a) Initially, the soliton is at rest between the control atoms which are both in the ground-state  $|g\rangle$ . The BEC atoms initially are described by the many-body state  $|\Phi_0\rangle$  with a single macroscopically occupied orbital. (b) A laser (arrows) targets the control atoms to bring them into a Rydberg excited state  $|R\rangle$ , but owing to the interaction blockade generates the entangled state shown. (c) We now initiate Rydberg dressing lasers (green) so that all atoms in the soliton (green shade in centre) acquire long-range interactions with the control atoms but not among themselves. (d) The resultant long-range potential (red solid line) is conditional on the state of the control atoms, which were in a superposition state. Hence, the superposition in electronic states of the control atoms is mapped onto a spatial superposition of the condensate soliton as shown with  $|\Phi_1\rangle$  implying the soliton has moved left and  $|\Phi_2\rangle$  that it has moved right. Green dashed lines indicate the initial soliton position.

matter wave soliton consisting of  $N$  atoms centered at  $x = 0$  with two tightly trapped atoms located at a distance  $d$ , e.g.,  $d = 1.5 \mu\text{m}$  on either side from the center of the soliton as sketched in Fig. 1.

We call these tightly trapped atoms “control atoms.” The distance between the control atoms  $2d$  is assumed to be less than the blockade radius  $R_b$  for a particular Rydberg state  $|R\rangle = |n_c, s\rangle$  with principal quantum number  $n_c$  and angular momentum  $l = 0$ . We assume that the control atoms can be coupled from their ground-state  $|g\rangle$  to  $|R\rangle$  with Rabi frequency

$\Omega_c$ , e.g., using a two-photon process. This may be experimentally realized by using laser beams and beam splitters to focus low waist coherent laser source on to the control atoms without affecting the soliton. To enable the control atoms to affect the soliton over the large range  $d$ , the atoms in the latter are dressed to a Rydberg state  $|r\rangle = |n_d, s\rangle$  with  $n_d \neq n_c$ . When attempting to excite the control atoms under blockade conditions, they can be brought into the entangled state  $|C\rangle = (|gR\rangle + |Rg\rangle)/\sqrt{2}$  with high fidelity [46,47], where  $|gR\rangle$  ( $|Rg\rangle$ ) indicates that the right (left) control atom is excited. It has been shown in Ref. [22] that the Rydberg dressed atoms interact with a Rydberg control atom through an effective potential of the shape,

$$U_{\text{eff}}(r, t) = V_0(t) \left[ 1 - \left( \frac{r_c}{r} \right)^6 \right]^{-1}, \quad (1)$$

where  $r$  is the distance between the impurity atom and the Rydberg dressed atom. The parameters governing the strength  $V_0$  and range  $r_c$  are given in terms of the underlying Rydberg interactions and dressing parameters in Appendix B. The potential (1) is sketched by solid red lines in Fig. 1(d), its strength  $V_0$  can be controlled in time through the intensity of dressing lasers.

The control atoms are tightly trapped in their respective positions by an external potential, whereas Bose atoms forming the soliton are untrapped along one direction. Hence, as the latter feel the effective potential  $U_{\text{eff}}(r, t)$ , they accelerate, setting the soliton into collective motion. Depending upon which control atom is excited, the soliton will either move towards the left or towards the right. The joint state of soliton and control atoms following this conditional acceleration of the soliton then becomes

$$|\Psi(t)\rangle = C_1(t) |Rg\rangle \otimes |\Phi_1(t)\rangle + C_2(t) |gR\rangle \otimes |\Phi_2(t)\rangle, \quad (2)$$

where  $|\Phi_{1,2}(t)\rangle$  are shown in Fig. 1 and its caption. After finally deexciting the control atoms again, we have generated a moving soliton in a superposition state given by  $|\Psi\rangle = (|\Phi_L\rangle + |\Phi_R\rangle)/\sqrt{2}$ , where  $|\Phi_L\rangle$ ,  $|\Phi_R\rangle$  indicate the left-moving soliton state  $|\Phi_1\rangle$  and right-moving soliton state  $|\Phi_2\rangle$ , respectively, after they have spatially separated and have negligible spatial overlap. The entire entanglement mapping sequence is sketched in Fig. 1.

It is clear that the conversion of the condensate soliton into the superposition state of two different locations  $|\Phi_L\rangle$  and  $|\Phi_R\rangle$  inherently cannot be described in the usual mean-field picture since the latter requires all bosons to occupy the same single-particle state. However since creation of the state  $|\Psi(t)\rangle$  involves the superposition of just two different types of dynamics, a multiconfigurational picture allowing two different highly occupied orbitals, each separately amenable to a mean-field picture, can capture the essentials if each of these orbitals is associated with a specific two-body state of the control atom pair. In the following, we discuss the accordingly customized variational approach for this type of dynamics, which can be classified as a much simplified version of the recently developed ML-MCTDHB method [57,61] that can be used to describe the beyond mean-field physics of multi-species Bose gases.

For successfully bringing the soliton into the mesoscopically entangled state, the entire process should be quantum

coherent. Hence, it is important to assess the strength of decoherence affecting the system. We expect the most important decoherence sources for the soliton to be one-, two-, and three-body loss of atoms, arising from interactions of condensate atoms with vacuum imperfections or stray photons, spin-changing collisions or inelastic collision between three condensate atoms [67]. When considering the soliton as an open quantum system, the loss of an atom can constitute a *measurement* of the system, leading to a collapse of the wave function and breaking the coherence of the mesoscopically entangled state [68,69]. All this will be explored in Sec. III.

### A. Two-species model

We first discuss the Hamiltonian of our system, which we split into three parts. One describing the dynamics of the control atoms  $\hat{H}_{\text{ctrl}}(t)$ , one for the bosonic atoms initially constituting the matter wave soliton  $\hat{H}_{\text{BEC}}$ , and the last one for interaction of control atoms with the soliton induced by Rydberg dressing  $\hat{H}_I(t)$ ,

$$\hat{H} = \hat{H}_{\text{ctrl}}(t) + \hat{H}_{\text{BEC}} + \hat{H}_I(t). \quad (3)$$

As described above, there are two control atoms which can be in a ground-state  $|g\rangle$  or Rydberg state  $|R\rangle$  under dipole blockade conditions. Thus, only the two-body states  $|0\rangle \equiv |gg\rangle$ ,  $|1\rangle \equiv |Rg\rangle$ , and  $|2\rangle \equiv |gR\rangle$  are available to them. We assume the control atoms to be tightly confined in the ground state of an optical trap, and, hence, no spatial dynamics is allowed for them. Coupling between these electronic states is possible when driving the  $|g\rangle \leftrightarrow |R\rangle$  transition with Hamiltonian,

$$\hat{H}_{\text{ctrl}}(t) = \frac{\Omega_c(t)}{\sqrt{2}} (|0\rangle\langle 1| + |0\rangle\langle 2| + \text{c.c.}) \otimes \mathbb{I}_{\mathcal{B}}, \quad (4)$$

where  $\Omega_c(t)$  is the effective Rabi frequency of that transition and we have included the  $\sqrt{2}$  enhancement of the many-body Rabi-frequency [46] and (c.c.) denotes the complex conjugate. We denote the Hilbert space for the control atoms by  $\mathcal{C}$  and for the Bose atoms by  $\mathcal{B}$  such that  $\mathbb{I}_{\mathcal{B}}$  denotes the identity in the space of the Bose atoms.

The Hamiltonian for  $N$  Bose atoms each with mass  $m$  is given by

$$\begin{aligned} \hat{H}_{\text{BEC}} = & \mathbb{I}_{\mathcal{C}} \otimes \sum_{i=1}^N \frac{\hat{p}_i^2}{2m} + \mathbb{I}_{\mathcal{C}} \otimes \sum_{i=1}^N V_{\text{ext}}(\hat{r}_i) \\ & + \mathbb{I}_{\mathcal{C}} \otimes \sum_{i,j=1, i \neq j}^N \frac{g}{2} \delta(\hat{r}_i - \hat{r}_j), \end{aligned}$$

where  $\hat{r}_i$  and  $\hat{p}_i$  are the position and momentum operators, respectively, of the  $i$ th atom,  $V_{\text{ext}}$  denotes an external potential and  $g = 4\pi\hbar^2 a/m$  is the usual contact interaction strength with  $s$ -wave scattering length  $a$ . The external potential will not be required for the scheme sketched in Fig. 1 but will be included in the derivation of the next section to widen the applicability of the results.

Finally the interaction Hamiltonian is written as

$$\hat{H}_I(t) = \sum_{i=0}^2 \left( |i\rangle\langle i| \otimes \sum_{j=1}^N V_{\text{int}}^{(i)}(\mathbf{x}_i - \hat{r}_j, t) \right), \quad (5)$$

where for  $i \in \{1, 2\}$  we have  $V_{\text{int}}^{(i)}(\mathbf{x}_i - \hat{r}_j, t) = U_{\text{eff}}(\mathbf{x}_i - \hat{r}_j, t)$  as the interaction potential between the BEC atoms and the control atoms at positions  $\mathbf{x}_i$ , see Eq. (1) and Fig. 1. For  $i = 0$  we define  $V_{\text{int}}^{(0)} \equiv 0$  for later convenience since there is no interaction between BEC atoms and the control atoms when both are in the ground state. The time dependence of the interaction potential is controlled via the intensity of the laser dressing the BEC atoms off-resonantly to Rydberg states.

### B. Variational multiorbital ansatz

The entanglement mapping sequence in Fig. 1 starts by transferring the control atoms from a product state into an entangled state. This entanglement is then mapped onto a fairly simply structured many-body state for the atoms initially constituting the soliton. To capture this sequence mathematically, we employ the following ansatz for the many-body wave function,

$$|\Psi(t)\rangle = C_0(t)|0\rangle \otimes |\Phi_0(t)\rangle + C_1(t)|1\rangle \otimes |\Phi_1(t)\rangle + C_2(t)|2\rangle \otimes |\Phi_2(t)\rangle, \quad (6)$$

where the  $|\Phi_i(t)\rangle$  still represent a many-body state, namely, of the Bose atoms in space  $\mathcal{B}$ . The coefficients  $C_i(t)$  are the probability amplitudes for each component of the superposition. Now for each  $|\Phi_i(t)\rangle$ , we assume the usual mean-field approach for a weakly interacting BEC, and write it in the position space representation as a product,

$$\langle \mathbf{r} | \Phi_i(t) \rangle = \Phi_i(\mathbf{r}, t) = \prod_{j=1}^N \phi_j(r_j, t), \quad (7)$$

where all the  $N$  particles occupy the same single-particle state  $\phi_i$ . Here  $\mathbf{r}$  denotes a vector  $\mathbf{r} = [r_1, \dots, r_N]^T$  with all atomic positions except the control atoms. States  $\phi_i(r_j, t)$  are normalized at all times  $\int dr_j |\phi_i(r_j, t)|^2 = 1$ .

Using the Hamiltonian in Eq. (3) and the ansatz in Eq. (6) with  $\Psi(\mathbf{r}, t) = \langle \mathbf{r} | \Psi(t) \rangle$ , we can write the action,

$$S = \int dt d^N \mathbf{r} \left\{ \Psi^*(\mathbf{r}, t) \left( \hat{H} - i\hbar \frac{\partial}{\partial t} \right) \Psi(\mathbf{r}, t) \right\} - \int dt \sum_{j=0}^2 \lambda_j \left( \int d^N \mathbf{r} \Phi_j^*(\mathbf{r}, t) \Phi_j(\mathbf{r}, t) - 1 \right), \quad (8)$$

where the  $\lambda_j$ 's are Lagrange multipliers ensuring the normalization of the many-body soliton wave-function  $\Phi_j(\mathbf{r}, t)$ . Importantly, the  $\Phi_j$  are *not* required to be orthogonal. From the minimization of this action with respect to the coefficients  $\{C_i(t)\}$  and single-particle wave-functions  $\{\phi_i(r, t)\}$  in Eq. (6), and exploiting the product forms in Eq. (7), we obtain our evolution equations as discussed in detail in Appendix A.

The one describing the coefficients  $C_i(t)$  becomes

$$i\hbar \frac{\partial}{\partial t} C_i(t) = \sum_{j=0, i \neq j}^2 C_j(t) \langle i | \hat{H}_{\text{ctrl}}(t) | j \rangle \mathcal{M}_{ij}(t)^N + N C_i(t) \int d\tilde{r} \left[ [V_{\text{ext}}(\tilde{r}) + V_{\text{int}}^{(i)}(\mathbf{x}_i - \tilde{r}, t)] \times |\phi_i(\tilde{r}, t)|^2 + \frac{g(N-1)}{2} |\phi_i(\tilde{r}, t)|^4 \right], \quad (9)$$

where  $\mathcal{M}_{ij}(t) = \int d\tilde{r} \phi_i^*(\tilde{r}, t) \phi_j(\tilde{r}, t)$  is the overlap integral between single-particle modes  $i$  and  $j$ . If  $\mathcal{M}_{ij}(t) < 1$ , the orbital attached to state  $|i\rangle$  cannot correctly represent the spatial wave function of condensate atoms earlier residing in  $|\Phi_j(t)\rangle$  after those underwent a transition from  $|j\rangle$  to  $|i\rangle$ . If there were a large number of many-body states multiplying  $|i\rangle$  in Eq. (6) that formed a basis,  $\mathcal{M}_{ij}(t)$  would ensure the selection of the appropriate spatial structure. Since this is not the case,  $\mathcal{M}_{ij}(t) < 1$  with  $\langle i | \hat{H}_{\text{ctrl}}(t) | j \rangle \neq 0$  signals a limitation of the present ansatz. We will restrict ourselves to scenarios where this does not occur. The second line in Eq. (9) simply describes the potential and interaction energy of the  $N$  bosons in single-particle state  $\phi_i$ .

The equation of motion of single-particle orbitals is

$$i\hbar \frac{\partial}{\partial t} \phi_i(r, t) = \sum_{j=0, i \neq j}^2 \left\{ \left[ \frac{C_j(t)}{C_i(t)} \langle i | \hat{H}_{\text{ctrl}}(t) | j \rangle \mathcal{M}_{ij}(t)^{N-1} \right] \times [\phi_j(r, t) - \phi_i(r, t) \mathcal{M}_{ij}(t)] \right\} + \hat{h}_i \phi_i(r, t) + V_{\text{int}}^{(i)}(\mathbf{x}_i - r, t) \phi_i(r, t) - \phi_i(r, t) \int d\tilde{r} \phi_i^*(\tilde{r}, t) [V_{\text{ext}}(\tilde{r}) \phi_i(\tilde{r}, t) + g(N-1) |\phi_i(\tilde{r}, t)|^2 \phi_i(\tilde{r}, t)] - \phi_i(r, t) \int d\tilde{r} \phi_i^*(\tilde{r}, t) V_{\text{int}}^{(i)}(\mathbf{x}_i - \tilde{r}, t) \phi_i(\tilde{r}, t), \quad (10)$$

where the operator  $\hat{h}_i$  acting on single-particle states is given by

$$\hat{h}_i = -\frac{\hbar^2}{2m} \nabla_r^2 + V_{\text{ext}}(\tilde{r}) + g(N-1) |\phi_i(\tilde{r}, t)|^2. \quad (11)$$

The approach adopted above can be viewed as a (much) simplified version of the ML-MCTDHB method [57–60], which is an advanced method to study the dynamics of multi-species ultracold atomic gases. It contains a component akin to basic MCTDHB [70,71], where  $N$  atoms in one of the species can be distributed among  $M$  orbitals in a dynamically evolving manner. Additionally for multiple species, their respective many-body wave functions are allowed to be in several different product states of these multiorbital superpositions. We confine ourselves to a case where all  $N$  atoms are in the same orbital, but this one may differ depending on the state of the second species. The justification for this will be discussed in detail at the end.

In Eqs. (9) and (10), the terms on the right-hand side involving integrals result in the usual complex phase oscillations of the  $C_i$  due to the action of the trapping potential on the soliton, the interparticle interaction of the BEC atoms and the phase imprinted on the orbital  $|\Phi_i\rangle$  by the control atoms. However, the more interesting dynamics occurs due to the off-diagonal parts represented by summations in the two integrals and are dependent on the coupling between the Rydberg states and the ground state of the control atoms. Without this coupling the coefficients corresponding the orbitals  $|\Phi_1\rangle$  and  $|\Phi_2\rangle$  would remain zero and as such the system would continue to remain in the initially occupied orbital  $|\Phi_0\rangle$ .

### C. Generation of mesoscopic spatial superposition state

We now employ the variational method above to model the procedure in Fig. 1 of bringing a BEC bright soliton into a mesoscopically entangled state by mapping Rydberg atomic entanglement onto it. Detailed parameters employed throughout the demonstration are given in Appendix B.

*Step (a).* The starting point at  $t < 0$  is a quasi-1D bright soliton of  $N = 400$  atoms of  $^{85}\text{Rb}$  with attractive interactions as their scattering length is tuned to  $a = -5.33 \times 10^{-9}$  m using a Feshbach resonance [40]. For a quasi-1D setting, the radial confinement must be much stronger than the axial one, hence, we neglect the latter. The radial trap frequency  $\omega_r$  then still affects the effective 1D interaction strength  $g = 2\hbar\omega_r a$ , whereas the three-dimensional (3D) interaction strength would have been  $g_{3D} = 4\pi\hbar^2 a/m$ .

As discussed before, the control atoms are tightly trapped and placed at a distance of  $d = 1.5 \mu\text{m}$  on each side of the center of the bright soliton. The total state of the system (6) at the beginning is  $|\Psi(t < 0)\rangle = |0\rangle \otimes |\Phi_0(t < 0)\rangle$ , where  $|\Phi_0(t < 0)\rangle$  is given by Eq. (7) with

$$\phi_0(r, t < 0) = \frac{1}{\sqrt{2\xi_0}} \text{sech}(r/\xi_0). \quad (12)$$

The scale  $\xi_0 = \hbar/(m\omega_r|a|N) = 0.4 \mu\text{m}$  is the condensate healing length.

Thus, at this point all  $N$  atoms form a BEC bright soliton, which is for now amenable to mean-field theory. In terms of our formalism in Sec. II B this initial state is described by  $C_0(0) = 1$ ,  $C_1(0) = C_2(0) = 0$ , and  $\phi_i(r, 0)$  for  $i \in \{0, 1, 2\}$  given by Eq. (12).

*Step (b).* The distance  $2d$  between the control atoms is within their mutual blockade radius  $R_b = (C_6^{RR}/\Omega_c)^{1/6}$ , assuming a van der Waals interaction with dispersion coefficient  $C_6^{RR}$  between two Rydberg atoms in a  $|R\rangle$  state. The blockade effectively removes the doubly excited-state  $|RR\rangle$  from the control atom Hilbert space, and upon driving Rydberg excitation with Rabi frequency  $\Omega_c = (6\sqrt{2}/\pi)$  MHz for a short-time  $t_{\text{excite}} = 2.3 \mu\text{s}$ , we can bring the control atoms into the entangled state  $(|Rg\rangle + |gR\rangle)/\sqrt{2}$ . The total system state is hence now  $|\Psi(t = t_{\text{excite}})\rangle = [(|1\rangle + |2\rangle)/\sqrt{2}] \otimes |\Phi_0(t = t_{\text{excite}})\rangle$ . We can explicitly model this step as shown in Fig. 2, using Eqs. (9) and (10), resulting in coefficients  $C_0 = 0$ ,  $C_1 = C_2 = 1/\sqrt{2}$ , while all  $\phi_i(r, t)$  remain unchanged since the soliton still is a stationary state of Eq. (10). Our simulation makes use of the ARK89 [72,73] adaptive step-size algorithm within the high-level language XMDS [74,75].

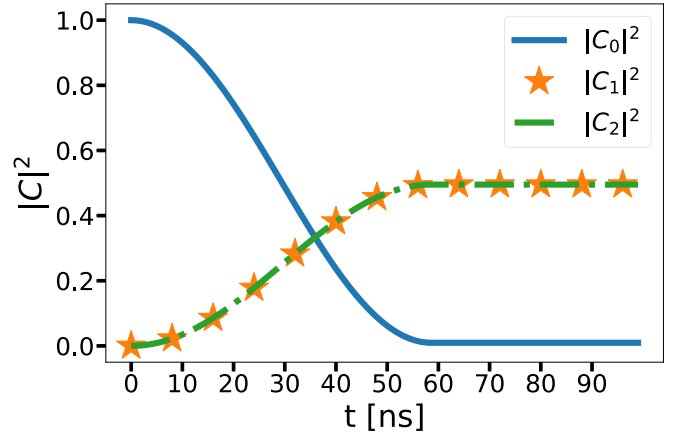


FIG. 2. Probability of finding the joint system of control atoms and Bose gas in the many-body states  $|0\rangle \otimes \Phi_0$  (blue solid line),  $|1\rangle \otimes \Phi_1$  (yellow star), and  $|2\rangle \otimes \Phi_2$  (green dashed line) according to Eqs. (9) and (10), during laser excitation of the control atoms from their ground state to a Rydberg excited state. This corresponds to step (b) in Fig. 1 and the description in the text. On this short timescale, the single-particle states  $\phi_j$  do not evolve significantly.

*Step (c).* Only at this point does one enable Rydberg dressing of the BEC soliton [22] for duration  $t_{\text{dress}} = 36 \mu\text{s}$  such that  $V_{\text{int}} \neq 0$  in Eq. (5). Dressing can be adiabatically enabled and disabled so that after  $t_{\text{dress}}$  all condensate atoms returned to their ground state. Importantly, since the interaction potential is centered on the particular control atom that is Rydberg excited, the potential  $V_{\text{int}}^{(i)}$  entering Eq. (10) is different for  $i = 1, 2$ , as sketched in panel (d) of Fig. 1, and the potential is absent for  $i = 0$ . This causes the soliton to feel an acceleration into different directions, conditional on the state of the control atom. At the end of this initial acceleration step, at  $t = t_{\text{excite}} + t_{\text{dress}}$ , the control atoms would ideally be again deexcited into  $|0\rangle = |gg\rangle$  by inverting step (b). We cannot explicitly model that step within the ansatz in Eq. (6) and will discuss this limitation and a possible remedy later.

*Step (d).* We finally allow free motion of the  $N$  Bose gas atoms for a duration  $t_{\text{mov}} = 2$  ms. As we can see in Fig. 3, in this step the superposition of Rydberg control atoms that we had generated in step (b) is finally converted into a superposition state where the entire soliton of  $N$  atoms has either arrived at a location near  $x_L \approx -1.5 \mu\text{m}$  in panel (a) or near  $x_R \approx +1.5 \mu\text{m}$  in panel (b). The two kinds of motion natu-

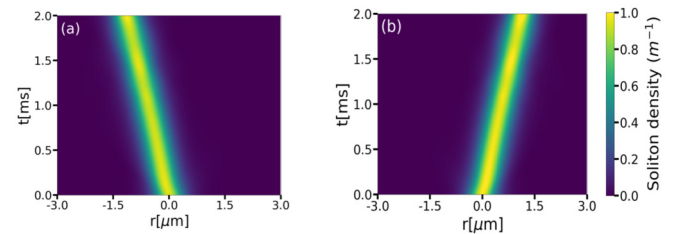


FIG. 3. Evolution of the individual soliton orbitals (a)  $|\phi_1|^2$  and (b)  $|\phi_2|^2$ . We can clearly see that owing to the initial acceleration in opposite directions due to interaction with Rydberg control atoms in a superposition state, the soliton finds itself in a superposition of two different modes of motion, through Eq. (6).

rally occur in one joint simulation via Eqs. (9) and (10), and allow identification of the many-body superposition character through Eq. (6). In terms of Eq. (6), the final state of the simulation at time  $t_{\text{end}} = t_{\text{excite}} + t_{\text{dress}} + t_{\text{mov}}$  is now

$$\begin{aligned} |\Psi(t_{\text{end}})\rangle &= C_1|1\rangle \otimes |\Phi_1(t_{\text{end}})\rangle + C_2(t)|2\rangle \otimes |\Phi_2(t_{\text{end}})\rangle, \\ &= \frac{1}{\sqrt{2}}(|1\rangle \otimes |\Phi_L\rangle + |2\rangle \otimes |\Phi_R\rangle), \end{aligned} \quad (13)$$

where the position space representation of  $|\Phi_{L,R}\rangle$  is  $\langle \mathbf{r} | \Phi_{L,R} \rangle = \prod_{j=1}^N \phi_{L,R}(r_j)$ . Here  $\phi_{L,R}$  represent the single-particle states  $\phi_{1,2}$  when they have significantly separated such that their overlap  $\int dr \phi_1^*(r)\phi_2(r) \ll 1$ .

At this point we have, thus, extended Ref. [22] by an explicit calculation of the entangling many-body dynamics yielding Eq. (13).

Prior to the period of free motion in step (d), the control atoms should be driven back in to their ground-state  $|0\rangle$  to disentangle them from the BEC and avoid decoherence through their spontaneous decay. This step cannot be modeled yet with the present ansatz since it would require the attachment of, at least, two orbitals to the  $|0\rangle$  state of the control atoms. We defer this extension to future work since providing the variational ansatz with further orbitals may cause convergence problems due to center-of-mass diffusion of the soliton [20,76,77]. Although our restriction to a single orbital per impurity state is, of course, also not a converged many-body theory, it is still expected to capture the essence of mesoscopically entangled state creation up to the point of control deexcitation.

Experimental proof of the mesoscopic superposition created as discussed here, would mainly have to distinguish it from two similar states: (i) a classical incoherent mixture of the left and right moving soliton, and (ii) a BEC that is split into two parts, one of which moves left and the other right. Possibility (ii) can be easily ruled out by simple absorption images which show only ever a single soliton moving either left or right in the mesoscopic superposition but would simultaneously contain two fragments if the BEC has been split. Ruling out (i) is more involved. One option is to place the soliton into a weak trap along the direction of motion and, thus, recombine the left and right moving parts of the wave function after half an oscillation period. In that case the mesoscopic superposition is heralded by fringes in the wave function for the center of mass [19,26,78]. During the initial time in which the superposition is getting created but not yet complete, one can also distinguish the superposition state from a mixture through features in single body densities as we discuss in Ref. [79]. The period for this corresponds to the first 5–10  $\mu\text{s}$  of step (c) above.

### III. DECOHERENCE OF MESOSCOPIC SPATIAL SUPERPOSITION STATE

Atoms in the mesoscopic superposition state generated above are not isolated but interact with their environment. Two important components of this interaction are collisions with residual uncondensed  $^{85}\text{Rb}$  atoms, as well as inelastic collisions within the condensate, which result in ejection of atoms from it and, hence, loss into the environment. Through

these, the many-body system discussed so far will decohere, and we expect the mesoscopic superposition state to be fragile. The loss of a single atom from such a state is known to lead to complete decoherence [68,69]. A detailed assessment of decoherence times is necessary for many practical uses of mesoscopic superposition states since any bounds on parameters for collapse models [7,8] can only arise if these affect the state prior to decoherence.

We can neglect the decoherence induced in the soliton during excitation of control atoms into the superposition state and Rydberg dressing of soliton atoms: The control atoms can be excited within tens of nanoseconds, much shorter than the timescale of loss processes in the BEC. Furthermore, the Rydberg dressing can operate far detuned with parameters listed in Appendix C so that the relative fraction of Rydberg state versus ground-state populations is of the order of  $1 \times 10^{-5}$ . This ensures that also spontaneous Rydberg decay during the dressing does not significantly affect the BEC on the relevant timescale of  $t_{\text{dress}} = 36 \mu\text{s}$  [80,81].

Since the duration of step (d) in Sec. II C in which the soliton moves freely, is orders of magnitude larger than the preceding steps, we conclude that decoherence is most relevant during this phase. The three major loss mechanisms in a BEC areas follows: (i) one-body loss due to collision of the condensate atoms with the atoms in the thermal cloud stray photons or vacuum imperfections, (ii) spin-flipping two-body interactions which results in the loss of condensate atoms from the trap and (iii) three-body losses due to inelastic collisions between the condensate atoms [67]. In what follows, we model our system using a Lindblad master equation and calculate the time required for the loss of an atom from the soliton. If this time is longer than the timescale of the experiments performed, then we can successfully create a macroscopic superposition state of the BEC which can be tested in experiments.

Note that the only contribution of thermal cloud interactions with condensate atoms that we consider here is when these cause an atom to be lost from the condensate. Another contribution could be decoherence from elastic collisions with thermal cloud atoms. It has been shown in Refs. [82,83] that the rate for the latter is, however, less than the former, hence, we have neglected it in our estimate.

#### A. Two-mode model and decoherence sources

To render the treatment of decoherence with a master equation tractable, we use a two-mode model describing the atom number dynamics with a restriction of spatial modes to a left- and a right-moving soliton mode that are spatially separated. These would correspond to  $\phi_1(\mathbf{r}, t)$  and  $\phi_2(\mathbf{r}, t)$  created after step (c) in Sec. II C. We utilize Fock states, where  $|0N\rangle$  represents all  $N$  atoms residing in the right-moving bright soliton mode and  $|N0\rangle$  correspondingly all atoms in the left-moving one. A decay of atoms from these states will cause incoherent population transfer to  $|0M\rangle$  and  $|M0\rangle$  with  $M < N$ . As described above, major loss processes are one-, two-, and three-body losses, which affect the density of the condensate  $n(t)$  as [84]

$$\frac{\partial}{\partial t}n(t) = -\kappa_1n(t) - \kappa_2n^2(t) - \kappa_3n^3(t), \quad (14)$$

where  $\kappa_1$ ,  $\kappa_2$ , and  $\kappa_3$  denote the one-, two-, and three-body loss rate coefficients, respectively. For  $^{85}\text{Rb}$  we take loss-rate coefficients  $\kappa_1 = 6 \times 10^{-3} \text{ s}^{-1}$  [62,63] for single-body loss,  $\kappa_2 = 2 \times 10^{-20} \text{ m}^3 \text{ s}^{-1}$  [64] for two-body loss, and  $\kappa_3 = 2 \times 10^{-40} \text{ m}^6 \text{ s}^{-1}$  [65,66] for three-body loss. Note, that these loss rates vary significantly among atomic species, isotopes, spin states, and in the case of one-body loss even experimental setup. Here we have chosen values for each loss rate that we consider representative.

We now model the decoherence arising from these loss processes with a Lindblad master equation for the density matrix of the system,

$$\hat{\rho}(t) = \sum_{k,l,m,n=0}^N \rho_{kl;mn}(t) |kl\rangle \langle mn|, \quad (15)$$

where  $|nm\rangle$  are Fock states in the two-mode model as discussed above.

Following Refs. [67,85], the starting point is the master equation,

$$\begin{aligned} \frac{d\hat{\rho}(t)}{dt} = & \frac{1}{i\hbar} [\hat{H}, \hat{\rho}(t)] + \int dr \sum_{n=1}^3 \left( \kappa_n [\hat{\Psi}(r)]^n \rho(t) [\hat{\Psi}^\dagger(r)]^n \right. \\ & \left. - \frac{\kappa_n}{2} \{ [\hat{\Psi}^\dagger(r)]^n [\hat{\Psi}(r)]^n, \rho(t) \} \right), \end{aligned} \quad (16)$$

where  $\hat{\Psi}(r)/\hat{\Psi}^\dagger(r)$  are field operators annihilating/creating a boson at a position  $r$  and the sum over  $n$ , thus, lists the three different loss processes. The Hamiltonian  $\hat{H}$  is as given in Eq. (3). In our simple model with two spatial modes, field operators become

$$\hat{\Psi}(r) = \phi_L(\mathbf{r})\hat{a} + \phi_R(\mathbf{r})\hat{b}, \quad (17)$$

where  $\phi_L(\mathbf{r})$  and  $\phi_R(\mathbf{r})$  represent the single-particle states for the sequence of entanglement mapping discussed in the previous section when the modes have separated. In other words,  $\phi_L(\mathbf{r}) = \phi_1(\mathbf{r})$  and  $\phi_R(\mathbf{r}) = \phi_2(\mathbf{r})$  at a time where  $\phi_{1,2}$  have reached negligible spatial overlap. Here  $\hat{a}$  and  $\hat{b}$  represent the annihilation operator for the left and the right modes, respectively. Insertion into Eq. (16) and projection onto  $|kl\rangle \langle mn|$  yields the evolution equation for the coefficients of the density-matrix  $\rho(t)_{kl;mn}$ ,

$$\begin{aligned} \frac{\partial \rho_{kl;mn}(t)}{\partial t} = & \mathcal{T}_{0;klmn} \rho_{kl;mn}(t) \\ & + \bar{\kappa}_1 [\mathcal{T}_{1;km} \rho_{(k+1)l;(m+1)n}(t) + \mathcal{T}_{1;ln} \rho_{k(l+1);m(n+1)}(t)] \\ & + \bar{\kappa}_2 [\mathcal{T}_{2;km} \rho_{(k+2)l;(m+2)n}(t) + \mathcal{T}_{2;ln} \rho_{k(l+2);m(n+2)}(t)] \\ & + \bar{\kappa}_3 [\mathcal{T}_{3;km} \rho_{(k+3)l;(m+3)n}(t) + \mathcal{T}_{3;ln} \rho_{k(l+3);m(n+3)}(t)]. \end{aligned} \quad (18)$$

The details of the derivation along with the expression for the effective loss-rate coefficients  $\bar{\kappa}_j$  and combinatorial factors  $\mathcal{T}$ s are presented in Appendix C. The  $\bar{\kappa}_j$  are based on the  $\kappa_j$  defined at the beginning of this section, but then also are sensitive to the soliton mode shape  $\phi_{L,R}(\mathbf{r})$ .

To significantly simplify the equation above, we have assumed that the overlap of the two modes vanishes

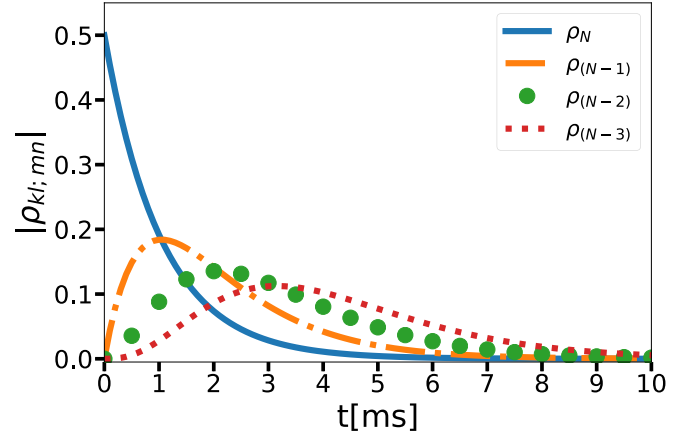


FIG. 4. Evolution of density-matrix components in the presence of atom losses, starting from a mesoscopically entangled state with  $N = 400$  atoms. The figure shows the modulus of selected components as a function of time. The (solid blue line) is  $\rho_N$ , corresponding to populations  $\rho_{0N;0N}$ ,  $\rho_{N0;N0}$ , and coherences  $\rho_{0N;N0}$  and  $\rho_{N0;0N}$ , which all have identical time evolution. We also show  $\rho_{N-1}$  (dashed-dot orange line),  $\rho_{N-2}$  (green circles), and  $\rho_{N-3}$  (dotted red line), where the elements  $\rho_i$  represent populations  $\rho_{0i;0i}$  and  $\rho_{i0;i0}$  for all  $i < N$ , the corresponding coherences  $\rho_{i0;0i}$  and  $\rho_{0i;i0}$  for  $i < N$  remain zero throughout.

$\int d^N \mathbf{r} \phi_L^*(\mathbf{r}) \phi_R(\mathbf{r}) = 0$ , which strictly means that the calculation is accurate only after the soliton in different branches of the superposition has moved by its width. In Fig. 3 this happens after approximately 0.5 ms, which makes this a good approximation for three-quarters of the relevant evolution period.

In the two-mode model, the mesoscopically entangled state of Sec. II C is represented by initial-state  $|\Psi(t=0)\rangle = (|N0\rangle + |0N\rangle)/\sqrt{2}$ , which gives a density matrix  $\hat{\rho}(t=0) = \frac{1}{2}(|N0\rangle \langle N0| + |N0\rangle \langle 0N| + |0N\rangle \langle N0| + |0N\rangle \langle 0N|)$ . Thus, the only initially nonvanishing elements of the density matrix are  $\rho_{N0;N0} = \rho_{N0;0N} = \rho_{0N;N0} = \rho_{0N;0N} = 1/2$ . This corresponds to the final result of Sec. II C if we have de-excited the control atoms. Equation (18) can in principle be solved analytically, using the thermofield technique [86], however, here we resort to a numerical solution which is shown in Fig. 4 for  $N = 400$ .

We show several selected density-matrix elements in Fig. 4. All those discussed above, which are initially nonzero, follow the same time evolution shown as the solid blue line. Except  $\rho_{0N;N0}$  and  $\rho_{N0;0N}$ , no coherence matrix elements become populated, hence, the density matrix no longer significantly contains coherences after roughly 3 ms. Instead we see a rise of population matrix elements for fewer atoms. For even later times density-matrix populations with even smaller atom content become populated, which we do not show.

To display the ramifications of this more clearly, we further calculate the average number of particles,

$$\langle \hat{N} \rangle = \sum_{k,l=0}^N \rho_{kl;kl}(t) (k+l), \quad (19)$$

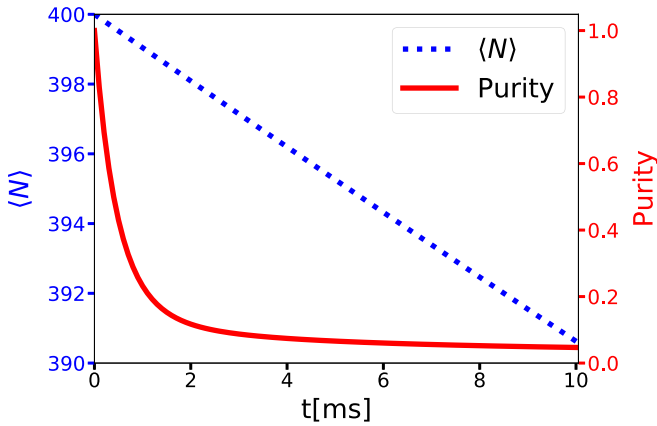


FIG. 5. Evolution of the average number of atoms  $\langle \hat{N} \rangle$  from Eq. (19) (dotted blue line) and purity from Eq. (20) (solid red line) of the system during the initial 10 ms. After a single atom is lost on average, around time 1 ms, the purity indicates almost complete decoherence to a mixed state.

and the purity of the density matrix as a function of time,

$$P = \text{Tr}[\hat{\rho}^2] = \sum_{k,l,m,n=0}^N |\rho_{kl,mn}(t)|^2 \quad (20)$$

shown in Fig. 5. We see that by the time the system has lost just one atom on average, the initially complete purity has almost entirely disappeared. After rapid initial decoherence, the purity decay slows significantly but it still continues to drop on much larger timescales. It is bounded from below by the dimension of the computational Hilbert space, which is  $d = N \times N$ , but this minimum is not approached yet for the times shown in Fig. 5. That the mesoscopically entangled state is decohered essentially at the time a single atom is lost is in accordance with earlier studies pertaining to BEC [23,87–89]. It has been discussed in [90] that the coherence of a mesoscopically entangled state decays exponentially with a timescale that will in our case be proportional to the number of atoms. Thus, the larger the number of atoms, the faster is the decoherence. This can be seen directly from Eq. (18) and the constant factors involved therein. As mentioned previously, for the parameters of our system the most prominent loss is the one-body loss. Therefore, looking at Eqs. (C2) and (C4), one can see that the loss coefficient contains the number of atoms  $N$  explicitly as well as implicitly in the factors  $k, l, m, n$ . One can then conclude from these equations that increasing the number of atoms in the system will accelerate the decay processes and, consequently, accelerate the fall of purity as well as the average atom number.

We have reproduced this phenomenology here for the specific parameters of the sequence in Fig. 1 in order to be able to accurately predict the expected decoherence timescale  $\tau \approx 1$  ms. The results here confirm the estimates given in Ref. [22]. By comparing simulations with different loss modes separately, we further identified single body loss as chief decoherence mechanism for the scenario here, using parameters listed above.

A point to note here, is that the period of free motion during which the superposition may decohere could be shortened by more intensive or longer dressing during step (c) in Sec. II C. This would impart a larger initial momentum kick onto the soliton and result in it reaching a sizable superposition distance faster. However, longer or stronger dressing would increase the probability of a spontaneous decay of either control or Rydberg dressed atoms, which are small for our present parameters.

#### IV. CONCLUSIONS AND OUTLOOK

We have studied the proposal of entanglement transfer from two Rydberg control atoms in the blockade regime onto a BEC bright soliton of Ref. [22] in more detail. Since Ref. [22] did focus on engineering the interactions (1) between dressed ground-state atoms and a Rydberg control atom, the proposal to create a mesoscopically entangled state relied on physical arguments without explicit simulation, and decoherence timescales were estimated. Here we have provided a formal theoretical framework for both these aspects, going beyond mean-field theory and considering the underlying many-body problem.

We confirm, that within a creation time of about  $40 \mu\text{s}$ , a BEC bright soliton containing about 400 atoms can be quantum entangled with two control atoms. This timescale is much less than the lifetime of the  $76S$  Rydberg state used in the scheme, which is of the order of few hundred microseconds [91]. Conditional on which of the two control atoms is Rydberg excited, the entanglement corresponds to the soliton having received a momentum kick in either of two opposite directions. After a further evolution time of about 1 ms, this momentum kick can be converted into a significant distance traveled so that the solitons finally find themselves in a superposition of two locations about  $3 \mu\text{m}$  apart.

Our model of this process is based on a restricted multi-configurational wave function with just three orbitals, tied to three control atom basis states. This is motivated by simplicity and physically by the structure of the interaction Hamiltonian between the BEC and the control atoms, which will to leading order create a state of this form. In principle the ansatz can be augmented to a larger number of superposition components, more orbitals per components and varying atom numbers per orbital, leading ultimately to the full fledged multicomponent MCTDHB form.

After the overlapping orbitals have separated, they undergo free motion. During that relatively long final phase of free motion, the mesoscopically entangled state may suffer decoherence, which we have explored comprehensively using a Lindblad master equation. We confirm the earlier estimate of decoherence time of about a few milliseconds.

The variational formalism discussed here could be useful also for other scenarios where entanglement between an initially pure Bose-Einstein condensed cloud and Rydberg impurity atoms is generated, for example, if a Rydberg impurity in a quantum superposition is embedded directly into the BEC [79], or if a multiatom Rydberg crystal [92–95] is generated within a BEC and then diagnosed through its interaction with it.



**ACKNOWLEDGMENTS**

We thank T. Busch and S. Chaturvedi for fruitful discussions and the Max-Planck Society for financial support under the MPG-IISER Partner Group Program.

**APPENDIX A: DERIVATION OF VARIATIONAL MULTIORBITAL EQUATIONS**

We here present the details of the derivation of evolution equations for the orbitals and coefficients in the ansatz of Eq. (6). The equations of motion are derived by minimization of the action,

$$S = \int dt d^N \mathbf{r} \left\{ \Psi^*(\mathbf{r}, t) \left( \hat{H} - i\hbar \frac{\partial}{\partial t} \right) \Psi(\mathbf{r}, t) \right\} - \int dt \sum_{j=0}^2 \lambda_j \left( \int d^N \mathbf{r} \Phi_j^*(\mathbf{r}, t) \Phi_j(\mathbf{r}, t) - 1 \right), \quad (\text{A1})$$

where  $\hat{H}$  is the Hamiltonian given by Eq. (3) and  $\lambda_j$ 's are the Lagrange multipliers. The second term on the right-hand side in the above equation ensures the normalization of the wave function at all times.

Inserting the ansatz in Eq. (6), we can split the resultant expression for the action into six terms,

$$S = \int dt d^N \mathbf{r} [T_1 + T_2 + T_3 + T_4 + T_5] - \int dt T_6, \quad (\text{A2})$$

which are

$$\begin{aligned} T_1 &= \sum_{i=0}^2 |C_i(t)|^2 \Phi_i^*(\mathbf{r}, t) \hat{H}_{\text{bcc}} \Phi_i(\mathbf{r}, t), \\ T_2 &= \sum_{i=1}^2 |C_i(t)|^2 |\Phi_i(\mathbf{r}, t)|^2 V_{\text{int}}^{(i)}(\mathbf{x}_i - r_j), \\ T_3 &= \sum_{i,j=0, i \neq j}^2 C_i^*(t) C_j(t) \langle i | \hat{H}_{\text{ctrl}}(t) | j \rangle \Phi_i^*(\mathbf{r}, t) \Phi_j(\mathbf{r}, t), \\ T_4 &= -i\hbar \sum_{i=0}^2 C_i^*(t) |\Phi_i(\mathbf{r}, t)|^2 \frac{\partial}{\partial t} C_i(t), \\ T_5 &= -i\hbar \sum_{i=0}^2 |C_i(t)|^2 \Phi_i^*(\mathbf{r}, t) \frac{\partial}{\partial t} \Phi_i(\mathbf{r}, t), \\ T_6 &= \sum_{j=0}^2 \lambda_j \left( \int d^N \mathbf{r} \Phi_j^*(\mathbf{r}, t) \Phi_j(\mathbf{r}, t) - 1 \right), \end{aligned} \quad (\text{A3})$$

where the integral measure for  $T_6$  is  $\int d^N \mathbf{r} = \int dr_1 dr_2 \cdots dr_N$  since  $\Phi_{ij}(\mathbf{r}, t)$ 's are many-body wave functions for  $N$  bosons. We now invoke the structure in Eq. (7) for each of them, hence, assuming they can be written as a product of the same single-particle states for all atoms in the orbital  $i$ . For this, we write  $\Phi_i(\mathbf{r}, t) = \prod_{j=1}^N \phi_i(r_j, t)$ . With this product ansatz and expanding  $\int d^N \mathbf{r}$ , we can simplify the above terms as discussed in the following.

Since the single-particle states are normalized as stated before, so are their many-body products and the expression  $|\Phi_i(\mathbf{r}, t)|^2$  in  $T_4$  is unity when integrated over all space. Many-body overlaps of the form  $\int d^N \mathbf{r} \Phi_i^*(\mathbf{r}, t) \Phi_j^*(\mathbf{r}, t)$  in  $T_3$  can be reexpressed as a  $N$ -fold product of identical single-particle overlaps, giving  $[\int d\tilde{r} \phi_i^*(\tilde{r}, t) \phi_j^*(\tilde{r}, t)]^N$ . Terms  $T_1$  and  $T_5$  have contributions of the form  $\int d^N \mathbf{r} \Phi_i^*(\mathbf{r}, t) \hat{O} \Phi_i(\mathbf{r}, t)$ , where  $\hat{O} \in \{\hat{h}_i, \frac{\partial}{\partial t}\}$  that simplify to a product of  $N$  identical single-particle integrals, yielding  $N \int d\tilde{r} \phi_i^*(\tilde{r}, t) \hat{O} \phi_i(\tilde{r}, t)$ , where  $\hat{O}$  is the single-particle operator acting on a single boson. Finally, the spatial integral over  $T_2$  contains  $\int d^N \mathbf{r} |\Phi_i(\mathbf{r}, t)|^2 V_{\text{int}}^{(i)}(\mathbf{x}_i - \mathbf{r})$ . When  $\Phi_i(\mathbf{r}, t)$  is written as a product of single-particle states, we get  $N \int dr |\phi_i(r, t)|^2 V_{\text{int}}^{(i)}(\mathbf{x}_i - r)$ . Considering these factors, the action in Eq. (A2) takes the form

$$\begin{aligned} S &= \int dt \left\{ N \sum_{i=0}^2 |C_i(t)|^2 \int d\tilde{r} \phi_i^*(\tilde{r}, t) \hat{h}_i[\phi_i] \phi_i(\tilde{r}, t) \right. \\ &\quad + N \sum_{i=1}^2 |C_i(t)|^2 \int d\tilde{r} |\phi_i(\tilde{r}, t)|^2 V_{\text{int}}^{(i)}(\mathbf{x}_i - \tilde{r}) \\ &\quad + \sum_{i,j=0, i \neq j}^2 C_i^*(t) C_j(t) \langle i | \hat{H}_{\text{ctrl}}(t) | j \rangle \left[ \int d\tilde{r} \phi_i^*(\tilde{r}, t) \phi_j(\tilde{r}, t) \right]^N \\ &\quad - i\hbar \sum_{i=0}^2 C_i^*(t) \frac{\partial}{\partial t} C_i(t) \\ &\quad - i\hbar N \sum_{i=0}^2 |C_i(t)|^2 \left[ \int d\tilde{r} \phi_i^*(\tilde{r}, t) \frac{\partial}{\partial t} \phi_i(\tilde{r}, t) \right] \\ &\quad \left. - \sum_{j=0}^2 \lambda_j \left[ \left( \int d\tilde{r} \phi_j^*(\tilde{r}, t) \phi_j(\tilde{r}, t) \right)^N - 1 \right] \right\}, \quad (\text{A4}) \end{aligned}$$

where the operator  $\hat{h}_i$  is the single-particle Hamiltonian for condensate atoms,

$$\hat{h}_i[\phi_i] = -\frac{\hbar^2}{2m} \nabla_r^2 + V_{\text{ext}}(r) + g(N-1) |\phi_i(r, t)|^2.$$

We now minimize the action above with respect to the single-particle states and the coefficients using functional derivatives, via  $\frac{\delta S}{\delta C_i^*} = i\hbar \frac{\partial C}{\partial t}$  and  $\frac{\delta S}{\delta \phi_i^*} = i\hbar \frac{\partial \phi}{\partial t}$ . From the resultant two equations, we still have to eliminate the Lagrange multiplier  $\lambda_i$ . By combining the two equations, we find that these have to satisfy

$$\begin{aligned} &\frac{\lambda_i}{|C_i(t)|^2} \left[ \int d\tilde{r} \phi_i^*(\tilde{r}, t) \phi_i(\tilde{r}, t) \right]^{N-1} \\ &= N_{\text{norm}}^i(t) \sum_{j=0, i \neq j}^2 \frac{C_j(t)}{C_i(t)} \langle i | \hat{H}_{\text{ctrl}}(t) | j \rangle \mathcal{M}_{ij}(t)^N \\ &\quad + N_{\text{norm}}^i(t) \int d\tilde{r} \phi_i^*(\tilde{r}, t) \hat{h}_i \phi_i(\tilde{r}, t) \\ &\quad + N_{\text{norm}}^i(t) \int d\tilde{r} \phi_i^*(\tilde{r}, t) V_{\text{int}}^{(i)}(\mathbf{x}_i - \tilde{r}) \phi_i(\tilde{r}, t) \\ &\quad - N_{\text{norm}}^i(t) \int i\hbar d\tilde{r} \phi_i^*(\tilde{r}, t) \frac{\partial}{\partial t} \phi_i(\tilde{r}, t), \quad (\text{A5}) \end{aligned}$$

where  $N_{\text{norm}}^i(t) = 1/\mathcal{M}_{ii}(t)$  and  $\mathcal{M}_{ij}(t) = \int d\tilde{r} \phi_i^*(\tilde{r}, t)\phi_j(\tilde{r}, t)$ . Using this expression for the Lagrange multipliers, we finally reach the evolution equations as

$$i\hbar \frac{\partial}{\partial t} C_i(t) = \sum_{j=0, i \neq j}^2 C_j(t) \langle i | \hat{H}_{\text{ctrl}}(t) | j \rangle \mathcal{M}_{ij}(t)^N + N C_i(t) \int d\tilde{r} \left[ (V_{\text{ext}}(\tilde{r}) + V_{\text{int}}^{(i)}(\mathbf{x}_i - \tilde{r}, t)) |\phi_i(\tilde{r}, t)|^2 + \frac{g(N-1)}{2} |\phi_i(\tilde{r}, t)|^4 \right]. \quad (\text{A6})$$

and

$$i\hbar \frac{\partial}{\partial t} \phi_i(r, t) = \sum_{j=0, i \neq j}^2 \left( \left\{ \frac{C_j(t)}{C_i(t)} \langle i | \hat{H}_{\text{ctrl}}(t) | j \rangle \times \left[ \int d\tilde{r} \phi_i^*(\tilde{r}, t)\phi_j(\tilde{r}, t) \right]^{N-1} \right\} \times \left[ \phi_j(r, t) - N_{\text{norm}}^i(t)\phi_i(r, t) \times \int d\tilde{r} \phi_i^*(\tilde{r}, t)\phi_j(\tilde{r}, t) \right] \right) + \hat{h}_i \phi_i(r, t) + V_{\text{int}}^{(i)}(\mathbf{x}_i - r)\phi_i(r, t) - N_{\text{norm}}^i(t)\phi_i(r, t) \int d\tilde{r} \phi_i^*(\tilde{r}, t)[V_{\text{ext}}(\tilde{r})\phi_i(\tilde{r}, t) + g(N-1)|\phi_i(\tilde{r}, t)|^2\phi_i(\tilde{r}, t)] - N_{\text{norm}}^i(t)\phi_i(r, t) \int d\tilde{r} \phi_i^*(\tilde{r}, t)V_{\text{int}}^{(i)}(\mathbf{x}_i - \tilde{r})\phi_i(\tilde{r}, t). \quad (\text{A7})$$

We see that Eq. (A6) implies that  $\frac{\partial}{\partial t} \sum_{i=0}^2 |C_i(t)|^2 = 0$  as expected and then Eq. (A7) yields  $\partial N_{\text{norm}}^i(t)/\partial t = 0$ . Since we always start with normalized single-particle orbitals  $\int dr |\phi_i(r, t=0)|^2 = 1$ , and these normalizations are preserved, we can just set  $N_{\text{norm}}^i(t) = 1$  for all  $i$ , which then yields Eq. (10) from Eq. (A7).

#### APPENDIX B: VALUES OF PARAMETERS USED FOR COMPUTATION

We consider a bright soliton with  $N = 400$  atoms of  $^{85}\text{Rb}$ , hence, the atomic mass is  $m = 1.419 \times 10^{-25}$  kg. Let the scattering length be tuned to  $a = -5.33 \times 10^{-9}$  m with a Feshbach resonance. The system is made effectively 1D by tightly trapping along the radial direction with trapping frequency  $\omega_r = 300\pi$  Hz and weak trapping along the axial direction with  $\omega_z = 100\pi$  Hz where we neglect the latter. The control atoms are very tightly trapped with a spread of  $\sigma = 0.05 \mu\text{m}$  and placed at a distance of  $d = 1.5 \mu\text{m}$  on each side of the center of the bright soliton.

The control atoms are coupled to a Rydberg S state with principal quantum number  $n_c = 76$  using a two-photon process with effective Rabi frequency  $\Omega_c = 6\sqrt{2}/(\pi)$  MHz. The Rydberg blockade radius under these conditions is given by  $R_b = \sqrt[6]{\frac{C_6^{RR}}{\Omega_c}} \sim 8.5 \mu\text{m}$  for  $C_6^{RR} \sim 10^3 \text{ GHz} \times \mu\text{m}^6$  for the Rydberg state 76S [97].

The atoms in the BEC soliton are dressed to a separate Rydberg S state with principal quantum number  $n_d = 55$ , assuming an effective Rabi frequency  $\Omega_{\text{bec}} = 3/(2\pi)$  MHz and detuning  $\Delta = -500/(2\pi)$  MHz. The Rydberg dressing causes an interaction between the soliton and the control atoms in the excited state with a potential given by  $V_{\text{int}}^{(i)}(\mathbf{x}_i - \mathbf{r}, t)$  which gives rise to (5). As mentioned there, for  $i \in \{1, 2\}$ ,  $V_{\text{int}}^{(i)}(\mathbf{x}_i - \mathbf{r}, t)$  is given by the effective potential  $U_{\text{eff}}(\mathbf{x}_i - \mathbf{r}, t) = \alpha^2 \Delta [1 - \sum_{j=1}^N \mathcal{Q}(\mathbf{x}_i - r_j)/\Delta]^{-1}$  where the bare van der Waals potential is  $\mathcal{Q}(\mathbf{x}_i - r_j) = C_6^{rR}/|\mathbf{x}_i - r_j|^6$  and the dressing parameter  $\alpha = \Omega_{\text{bec}}/(2\Delta)$  [22]. The position of the control atom is denoted by  $\mathbf{x}_i$  and the position of the dressed atom by  $r_j$ . Detailed choices for all these parameters are given in Table I.

#### APPENDIX C: CALCULATION OF EFFECTIVE LOSS RATES

Using Eq. (16), we can find the master equation for elements of the density matrix using the ansatz given in Eq. (17) and inserting the ansatz for single-particle states for particles in orbitals  $\Phi_L(\mathbf{r}, t)$  and  $\Phi_R(\mathbf{r}, t)$ , respectively, as  $\phi_L(r, t) = (1/\sqrt{2\xi_0})\text{sech}[(r+r_0)/\xi_0]$  and  $\phi_R(r, t) = (1/\sqrt{2\xi_0})\text{sech}[(r-r_0)/\xi_0]$  since we are considering the bright soliton solution of the BEC. This would give us the equation,

$$\begin{aligned} \frac{\partial \rho_{kl;mn}}{\partial t} = & \mathcal{T}_{0;klmn} \rho_{kl;mn} \\ & + \bar{\kappa}_1 \mathcal{T}_{1;km} \rho_{(k+1)l; (m+1)n} + \bar{\kappa}_1 \mathcal{T}_{1;ln} \rho_{k(l+1); m(n+1)} \\ & + \bar{\kappa}_{2,L} \mathcal{T}_{2;km} \rho_{(k+2)l; (m+2)n} + \bar{\kappa}_{2,R} \mathcal{T}_{2;ln} \rho_{k(l+2); m(n+2)} \\ & + \bar{\kappa}_{3,L} \mathcal{T}_{3;km} \rho_{(k+3)l; (m+3)n} + \bar{\kappa}_{3,R} \mathcal{T}_{3;ln} \rho_{k(l+3); m(n+3)}. \end{aligned} \quad (\text{C1})$$

where the density matrix elements  $\rho_{kl;mn}$  are time dependent. The coefficients in the equation above are given as follows in Eqs. (C2)–(C7). The coefficients involved in diagonal terms are

$$\begin{aligned} \mathcal{T}_{0;klmn} = & \left[ \frac{1}{i\hbar} \left( \bar{E}_L(k-m) + \bar{E}_R(l-n) \right. \right. \\ & + \frac{g}{2} \bar{\rho}_L^2 \{k(k-1) - m(m-1)\} \\ & \left. \left. + \frac{g}{2} \bar{\rho}_R^2 \{l(l-1) - n(n-1)\} \right) \right] \\ & - \frac{1}{2} \kappa_1 (k+l+m+n) \\ & - \frac{1}{2} \kappa_2 (k(k-1)\bar{\rho}_L^2 + m(m-1)\bar{\rho}_L^2 \\ & + l(l-1)\bar{\rho}_R^2 + n(n-1)\bar{\rho}_R^2) \end{aligned}$$

TABLE I. A tabular representation for the parameters and their values or expressions used in the simulation.

PARAMETER	EXPRESSION	VALUE/EXPRESSION
Number of Rb-85 atoms	$N$	400
Mass of Rb 85 atoms	$m$	$1.419 \times 10^{-25}$ kg
$s$ -wave scattering length	$a$	$-5.33 \times 10^{-9}$ m
External trap frequencies for BEC	$(\omega_r, \omega_z)$	$(300\pi, 100\pi)$ Hz
Spread of control atoms	$\sigma$	$0.05 \mu\text{m}$
Distance between control atoms	$2d$	$3 \mu\text{m}$
Rydberg state to which the control atoms are coupled	$n_c$	76S
Rabi frequency for control atom excitation	$\Omega_c$	$(6\sqrt{2}/\pi)$ MHz
Blockade radius for control atoms	$R_b = \sqrt[6]{\frac{C_6^{RR}}{\Omega_c}} \sim 8.5 \mu\text{m}$	$8.5 \mu\text{m}$
Rydberg state to which BEC atoms are dressed	$n_d$	55S
Rabi frequency for BEC atom dressing	$\Omega_{\text{bec}}$	$3/(2\pi)$ MHz
Detuning for dressing excitation	$\Delta$	$-500/(2\pi)$ MHz
Dressing parameter	$\alpha = \Omega_{\text{bec}}/(2\Delta)$	$-3 \times 10^{-3}$
$C_6$ coefficient for interaction between two atoms in a 76S Rydberg state	$C_6^{RR}$	$10^3$ GHz $\times \mu\text{m}^6$
$C_6$ coefficient for interaction between control atom in a 76S Rydberg state and BEC atoms dressed to a 55S Rydberg state	$C_6^{rR}$	$3$ GHz $\times \mu\text{m}^6$
Effective interaction potential between control atom ( $i$ ) and Rydberg dressed BEC atoms ( $j$ )	$U_{\text{eff}}(\mathbf{x}_i - \mathbf{r}, t)$	$\alpha^2 \Delta [1 - \sum_{j=1}^N \frac{C_6^{rR}}{( \mathbf{x}_i - \mathbf{r}_j ^6 \Delta)}]^{-1}$

$$\begin{aligned}
 & -\frac{1}{2} \kappa_3 (k(k-1)(k-2)\overline{\rho_L^3} + m(m-1)(m-2)\overline{\rho_L^3} \\
 & + l(l-1)(l-2)\overline{\rho_R^3} + n(n-1)(n-2)\overline{\rho_R^3}) \Big], \quad (\text{C2})
 \end{aligned}$$

where  $\overline{E}_{L/R}$ ,  $\overline{\rho_{L/R}^2}$ , and  $\overline{\rho_{L/R}^3}$  are defined in Eq. (C7). Note that for the particular problem that we look at over here,  $\overline{E}_L = \overline{E}_R$ ,  $\overline{\rho_L^2} = \overline{\rho_R^2}$ , and  $\overline{\rho_L^3} = \overline{\rho_R^3}$ . However, we have kept these terms distinct in the expression above to demonstrate the origin of terms. Next, the terms which connect the coefficients in the density matrix to coefficients separated by loss of one boson are

$$\begin{aligned}
 \mathcal{T}_{1;km} &= N\sqrt{(k+1)(m+1)}, \\
 \mathcal{T}_{1;ln} &= N\sqrt{(l+1)(n+1)}. \quad (\text{C3})
 \end{aligned}$$

Similarly, the terms which connect the coefficients of the density matrix to coefficients separated by the loss of two bosons are

$$\begin{aligned}
 \mathcal{T}_{2;km} &= N^2\sqrt{(k+1)(k+2)(m+1)(m+2)}, \\
 \mathcal{T}_{2;ln} &= N^2\sqrt{(l+1)(l+2)(n+1)(n+2)}. \quad (\text{C4})
 \end{aligned}$$

and lastly the terms which connect the coefficients of the density matrix to coefficients separated by the loss of three bosons are

$$\mathcal{T}_{3;km} = N^3\sqrt{(k+1)(k+2)(k+3)(m+1)(m+2)(m+3)},$$

$$\mathcal{T}_{3;ln} = N^3\sqrt{(l+1)(l+2)(l+3)(n+1)(n+2)(n+3)}. \quad (\text{C5})$$

In the above expressions, the coefficients  $N_{L/R}$  are defined due to the symmetry of the system at hand as

$$\begin{aligned}
 \overline{E}_L &= \int dr \phi_L^*(r) \hat{h}_f \psi_L(r) \\
 &= \int dr \phi_R^*(r) \hat{h}_f \phi_R(r) = \overline{E}_R, \\
 \overline{\rho_L^2} &= \int dr |\phi_L(r)|^4 \\
 &= \int dr |\phi_R(r)|^4 = \overline{\rho_R^2}, \\
 \overline{\rho_L^3} &= \int dr |\phi_L(r)|^6 \\
 &= \int dr |\phi_R(r)|^6 = \overline{\rho_R^3}, \quad (\text{C6})
 \end{aligned}$$

where  $\hat{h}_f = -(\hbar^2/2m)\nabla_r^2 + V_{\text{ext}}(r)$  in the above expression is the single-particle Hamiltonian for noninteracting bosons and the notation  $\overline{\rho^2}$  indicates a squared density averaged over the soliton mode. Finally, the redefined loss coefficients used in Eq. (18) and Eq. (C1) are given by

$$\begin{aligned}
 \bar{\kappa}_1 &= \kappa_1, \quad \bar{\kappa}_2 = \bar{\kappa}_{2,L/R} = \overline{\rho_{L/R}^2} \kappa_2, \quad (\text{C7}) \\
 \bar{\kappa}_3 &= \bar{\kappa}_{3,L/R} = \overline{\rho_{L/R}^3} \kappa_3.
 \end{aligned}$$

[1] M. A. Schlosshauer, in *Decoherence: and the Quantum-to-Classical Transition*, edited by A. C. Elitzur, M. P. Silverman, J. Tuszynski, R. Vass, and H. D. Zeh, the Frontiers Collection (Springer, Berlin, 2007).

[2] E. Joos, H. D. Zeh, C. Kiefer, D. J. Giulini, J. Kupsch, and I.-O. Stamatescu, *Decoherence and the Appearance of a Classical World in Quantum Theory* (Springer, Berlin, 2013).

[3] W. H. Zurek, *Rev. Mod. Phys.* **75**, 715 (2003).

- [4] A. Zavatta, S. Viciani, and M. Bellini, *Science* **306**, 660 (2004).
- [5] K. Modi, A. Brodutch, H. Cable, T. Paterek, and V. Vedral, *Rev. Mod. Phys.* **84**, 1655 (2012).
- [6] S. Haroche, *Rev. Mod. Phys.* **85**, 1083 (2013).
- [7] A. Bassi, K. Lochan, S. Satin, T. P. Singh, and H. Ulbricht, *Rev. Mod. Phys.* **85**, 471 (2013).
- [8] O. Romero-Isart, *Phys. Rev. A* **84**, 052121 (2011).
- [9] F. Fröwis, P. Sekatski, W. Dür, N. Gisin, and N. Sangouard, *Rev. Mod. Phys.* **90**, 025004 (2018).
- [10] M. Arndt, O. Nairz, J. Vos-Andreae, C. Keller, G. Van der Zouw, and A. Zeilinger, *Nature (London)* **401**, 680 (1999).
- [11] S. Gerlich, S. Eibenberger, M. Tomandl, S. Nimmrichter, K. Hornberger, P. J. Fagan, J. Tüxen, M. Mayor, and M. Arndt, *Nat. Commun.* **2**, 263 (2011).
- [12] S. Eibenberger, S. Gerlich, M. Arndt, M. Mayor, and J. Tüxen, *Phys. Chem. Chem. Phys.* **15**, 14696 (2013).
- [13] C. H. Van Der Wal, A. Ter Haar, F. Wilhelm, R. Schouten, C. Harmans, T. Orlando, S. Lloyd, and J. Mooij, *Science* **290**, 773 (2000).
- [14] A. Omran, H. Levine, A. Keesling, G. Semeghini, T. T. Wang, S. Ebadi, H. Bernien, A. S. Zibrov, H. Pichler, S. Choi *et al.*, *Science* **365**, 570 (2019).
- [15] T. Monz, P. Schindler, J. T. Barreiro, M. Chwalla, D. Nigg, W. A. Coish, M. Harlander, W. Hänsel, M. Hennrich, and R. Blatt, *Phys. Rev. Lett.* **106**, 130506 (2011).
- [16] D. Leibfried, E. Knill, S. Seidelin, J. Britton, R. B. Blakestad, J. Chiaverini, D. B. Hume, W. M. Itano, J. D. Jost, C. Langer *et al.*, *Nature (London)* **438**, 639 (2005).
- [17] D. Kleckner, I. Pikovski, E. Jeffrey, L. Ament, E. Eliel, J. Van Den Brink, and D. Bouwmeester, *New J. Phys.* **10**, 095020 (2008).
- [18] K. Tara, G. S. Agarwal, and S. Chaturvedi, *Phys. Rev. A* **47**, 5024 (1993).
- [19] S. Möbius, M. Genkin, A. Eisfeld, S. Wüster, and J.-M. Rost, *Phys. Rev. A* **87**, 051602(R) (2013).
- [20] A. Sreedharan, S. Choudhury, R. Mukherjee, A. Streltsov, and S. Wüster, *Phys. Rev. A* **101**, 043604 (2020).
- [21] A. I. Streltsov, O. E. Alon, and L. S. Cederbaum, *Phys. Rev. A* **80**, 043616 (2009).
- [22] R. Mukherjee, C. Ates, W. Li, and S. Wüster, *Phys. Rev. Lett.* **115**, 040401 (2015).
- [23] J. I. Cirac, M. Lewenstein, K. Mølmer, and P. Zoller, *Phys. Rev. A* **57**, 1208 (1998).
- [24] L. Pezze, M. Gessner, P. Feldmann, C. Klempt, L. Santos, and A. Smerzi, *Phys. Rev. Lett.* **123**, 260403 (2019).
- [25] D. Gordon and C. M. Savage, *Phys. Rev. A* **59**, 4623 (1999).
- [26] C. Weiss and Y. Castin, *Phys. Rev. Lett.* **102**, 010403 (2009).
- [27] L. Pezze, A. Smerzi, M. K. Oberthaler, R. Schmied, and P. Treutlein, *Rev. Mod. Phys.* **90**, 035005 (2018).
- [28] T. Mežnaršič, T. Arh, J. Brence, J. Pišljarič, K. Gosar, Ž. Gosar, R. Žitko, E. Zupanič, and P. Jeglič, *Phys. Rev. A* **99**, 033625 (2019).
- [29] P. J. Everitt, M. A. Sooriyabandara, M. Guasoni, P. B. Wigley, C. H. Wei, G. D. McDonald, K. S. Hardman, P. Manju, J. D. Close, C. C. N. Kuhn, S. S. Szigeti, Y. S. Kivshar, and N. P. Robins, *Phys. Rev. A* **96**, 041601(R) (2017).
- [30] G. D. McDonald, C. C. N. Kuhn, K. S. Hardman, S. Bennetts, P. J. Everitt, P. A. Altin, J. E. Debs, J. D. Close, and N. P. Robins, *Phys. Rev. Lett.* **113**, 013002 (2014).
- [31] S. Lepoutre, L. Fouché, A. Boissé, G. Berthet, G. Salomon, A. Aspect, and T. Bourdel, *Phys. Rev. A* **94**, 053626 (2016).
- [32] P. Medley, M. A. Minar, N. C. Cizek, D. Berryrieser, and M. A. Kasevich, *Phys. Rev. Lett.* **112**, 060401 (2014).
- [33] A. L. Marchant, T. P. Billam, T. P. Wiles, M. M. H. Yu, S. A. Gardiner, and S. L. Cornish, *Nat. Commun.* **4**, 1865 (2013).
- [34] A. L. Marchant, T. P. Billam, M. M. H. Yu, A. Rakonjac, J. L. Helm, J. Polo, C. Weiss, S. A. Gardiner, and S. L. Cornish, *Phys. Rev. A* **93**, 021604(R) (2016).
- [35] J. H. V. Nguyen, P. Dyke, D. Luo, B. A. Malomed, and R. G. Hulet, *Nat. Phys.* **10**, 918 (2014).
- [36] J. H. V. Nguyen, D. Luo, and R. G. Hulet, *Science* **356**, 422 (2017).
- [37] S. L. Cornish, S. T. Thompson, and C. E. Wieman, *Phys. Rev. Lett.* **96**, 170401 (2006).
- [38] B. Eiermann, T. Anker, M. Albiez, M. Taglieber, P. Treutlein, K.-P. Marzlin, and M. K. Oberthaler, *Phys. Rev. Lett.* **92**, 230401 (2004).
- [39] K. E. Strecker, G. B. Partridge, A. G. Truscott, and R. G. Hulet, *Nature (London)* **417**, 150 (2002).
- [40] L. Khaykovich, F. Schreck, G. Ferrari, T. Bourdel, J. Cubizolles, L. D. Carr, Y. Castin, and C. Salomon, *Science* **296**, 1290 (2002).
- [41] Y. S. Kivshar and G. P. Agrawal, *Optical Solitons: From Fibers to Photonic Crystals* (Academic, San Diego, 2003).
- [42] C. J. Pethick and H. Smith, *Bose-Einstein Condensation in Dilute Gases* (Cambridge University Press, Cambridge, UK, 2002).
- [43] K. E. Strecker, G. B. Partridge, A. G. Truscott, and R. G. Hulet, *New J. Phys.* **5**, 73 (2003).
- [44] T. F. Gallagher, *Rydberg Atoms* (Cambridge University Press, Cambridge, UK, 2005), Vol. 3.
- [45] T. Gallagher, *Rep. Prog. Phys.* **51**, 143 (1988).
- [46] A. Gaëtan, Y. Miroshnychenko, T. Wilk, A. Chotia, M. Viteau, D. Comparat, P. Pillet, A. Browaeys, and P. Grangier, *Nat. Phys.* **5**, 115 (2009).
- [47] E. Urban, T. A. Johnson, T. Henage, L. Isenhower, D. Yavuz, T. Walker, and M. Saffman, *Nat. Phys.* **5**, 110 (2009).
- [48] Y.-Y. Jau, A. Hankin, T. Keating, I. Deutsch, and G. Biedermann, *Nat. Phys.* **12**, 71 (2016).
- [49] J. B. Balewski, A. T. Krupp, A. Gaj, S. Hofferberth, R. Löw, and T. Pfau, *New J. Phys.* **16**, 063012 (2014).
- [50] J. E. Johnson and S. L. Rolston, *Phys. Rev. A* **82**, 033412 (2010).
- [51] S. Wüster, C. Ates, A. Eisfeld, and J. Rost, *New J. Phys.* **13**, 073044 (2011).
- [52] N. Henkel, R. Nath, and T. Pohl, *Phys. Rev. Lett.* **104**, 195302 (2010).
- [53] L. Santos, G. V. Shlyapnikov, P. Zoller, and M. Lewenstein, *Phys. Rev. Lett.* **85**, 1791 (2000).
- [54] F. Maucher, N. Henkel, M. Saffman, W. Królikowski, S. Skupin, and T. Pohl, *Phys. Rev. Lett.* **106**, 170401 (2011).
- [55] J. Honer, H. Weimer, T. Pfau, and H. P. Büchler, *Phys. Rev. Lett.* **105**, 160404 (2010).
- [56] G. Pupillo, A. Micheli, M. Boninsegni, I. Lesanovsky, and P. Zoller, *Phys. Rev. Lett.* **104**, 223002 (2010).
- [57] S. Krönke, L. Cao, O. Vendrell, and P. Schmelcher, *New J. Phys.* **15**, 063018 (2013).
- [58] R. Schmitz, S. Krönke, L. Cao, and P. Schmelcher, *Phys. Rev. A* **88**, 043601 (2013).

- [59] L. Cao, S. Krönke, O. Vendrell, and P. Schmelcher, *J. Chem. Phys.* **139**, 134103 (2013).
- [60] J. M. Schurer, P. Schmelcher, and A. Negretti, *Phys. Rev. A* **90**, 033601 (2014).
- [61] M. R. Ebgha, S. Saeidian, P. Schmelcher, and A. Negretti, *Phys. Rev. A* **100**, 033616 (2019).
- [62] E. A. Burt, R. W. Ghrist, C. J. Myatt, M. J. Holland, E. A. Cornell, and C. E. Wieman, *Phys. Rev. Lett.* **79**, 337 (1997).
- [63] L. A. Zundel, J. M. Wilson, N. Malvania, L. Xia, J.-F. Riou, and D. S. Weiss, *Phys. Rev. Lett.* **122**, 013402 (2019).
- [64] J. L. Roberts, N. R. Claussen, S. L. Cornish, and C. E. Wieman, *Phys. Rev. Lett.* **85**, 728 (2000).
- [65] C. M. Savage, N. P. Robins, and J. J. Hope, *Phys. Rev. A* **67**, 014304 (2003).
- [66] P. A. Altin, G. R. Dennis, G. D. McDonald, D. Döring, J. E. Debs, J. D. Close, C. M. Savage, and N. P. Robins, *Phys. Rev. A* **84**, 033632 (2011).
- [67] A. Sinatra and Y. Castin, *Eur. Phys. J. D* **4**, 247 (1998).
- [68] Y. P. Huang and M. G. Moore, *Phys. Rev. A* **73**, 023606 (2006).
- [69] D. Lombardo and J. Twamley, *Sci. Rep.* **5**, 13884 (2015).
- [70] O. E. Alon, A. I. Streltsov, and L. S. Cederbaum, *Phys. Rev. A* **77**, 033613 (2008).
- [71] A. U. J. Lode, *Phys. Rev. A* **93**, 063601 (2016).
- [72] W. H. Press and S. A. Teukolsky, *Comput. Phys.* **6**, 188 (1992).
- [73] W. H. Press, S. A. Teukolsky, W. T. Vetterling, and B. P. Flannery, *Numerical Recipes: The Art of Scientific Computing*, 3rd. ed. (Cambridge University Press, Cambridge, UK, 2007).
- [74] G. R. Dennis, J. J. Hope, and M. T. Johnsson, *Comput. Phys. Comm.* **184**, 201 (2013).
- [75] The SE and Tully's algorithm were both implemented in the high-level simulation language XMDS [74,96].
- [76] J. G. Cosme, C. Weiss, and J. Brand, *Phys. Rev. A* **94**, 043603 (2016).
- [77] C. Weiss, S. A. Gardiner, and H.-P. Breuer, *Phys. Rev. A* **91**, 063616 (2015).
- [78] B. Gertjerenken, *Phys. Rev. A* **88**, 053623 (2013).
- [79] S. Rammohan, S. Tiwari, A. Mishra, A. Pendse, A. K. Chauhan, R. Nath, A. Eisfeld, and S. Wüster, *arXiv:2011.11022* (2020).
- [80] J. A. Aman, B. J. DeSalvo, F. B. Dunning, T. C. Killian, S. Yoshida, and J. Burgdörfer, *Phys. Rev. A* **93**, 043425 (2016).
- [81] M. Płodzień, G. Lochead, J. de Hond, N. J. van Druten, and S. Kokkelmans, *Phys. Rev. A* **95**, 043606 (2017).
- [82] M. Bilardello, Heating effects and localization mechanism in cold Bose gases, Ph.D. thesis, Università degli Studi di Trieste, 2017.
- [83] A. Schelle, Environment-induced dynamics in a dilute Bose-Einstein condensate, Ph.D. thesis, Université Pierre et Marie Curie-Paris VI, 2009.
- [84] J. L. Roberts, Bose-Einstein condensates with tunable atom-atom interactions: The first experiments with 85Rb BECs, Doctoral dissertation, University of Colorado, 2001.
- [85] M. W. Jack, *Phys. Rev. Lett.* **89**, 140402 (2002).
- [86] S. Chaturvedi and V. Srinivasan, *Phys. Rev. A* **43**, 4054 (1991).
- [87] M. Brune, E. Hagley, J. Dreyer, X. Maître, A. Maali, C. Wunderlich, J. M. Raimond, and S. Haroche, *Phys. Rev. Lett.* **77**, 4887 (1996).
- [88] K. Pawłowski, M. Fadel, P. Treutlein, Y. Castin, and A. Sinatra, *Phys. Rev. A* **95**, 063609 (2017).
- [89] W. H. Zurek, *Phys. Today* **44**(10), 36 (1991).
- [90] P. J. Y. Louis, P. M. R. Brydon, and C. M. Savage, *Phys. Rev. A* **64**, 053613 (2001).
- [91] I. I. Beterov, I. I. Ryabtsev, D. B. Tretyakov, and V. M. Entin, *Phys. Rev. A* **79**, 052504 (2009).
- [92] T. Pohl, E. Demler, and M. D. Lukin, *Phys. Rev. Lett.* **104**, 043002 (2010).
- [93] R. M. W. van Bijnen, S. Smit, K. A. H. van Leeuwen, E. J. D. Vredenburg, and S. J. J. M. F. Kokkelmans, *J. Phys. B: At., Mol. Opt. Phys.* **44**, 184008 (2011).
- [94] P. Schauß, J. Zeiher, T. Fukuhara, S. Hild, M. Cheneau, T. Macrì, T. Pohl, I. Bloch, and C. Groß, *Science* **347**, 1455 (2015).
- [95] P. Schauß, M. Cheneau, M. Endres, T. Fukuhara, S. Hild, A. Omran, T. Pohl, C. Gross, S. Kuhr, and I. Bloch, *Nature (London)* **491**, 87 (2012).
- [96] G. R. Dennis, J. J. Hope, and M. T. Johnsson, <http://www.xmnds.org/>
- [97] T. Gould and T. Bucko, *J. Chem. Theory Comput.* **12**, 3603 (2016).